Impulsive sound reflection from an absorptive and dispersive planar boundary

Chee-Heun Lam, Bert Jan Kooij,[a] and Adrianus T. De Hoop
Laboratory of Electromagnetic Research, Faculty of Electrical Engineering, Mathematics and Computer Science, Delft University of Technology, 4 Mekelweg, 2628 CD Delft, The Netherlands

(Received 17 July 2003; revised 9 April 2004; accepted 6 May 2004)

The impulsive sound reflection from a planar boundary with absorptive and dispersive properties is investigated. The acoustic properties of the boundary are modeled via a local impedance transfer function whose complex frequency domain representation is taken to be a Padé (2,2) expression. The coefficients in this representation are matched to frequency domain acoustic wave reflection measurements. With the aid of the Cagniard–De Hoop method, a closed-form space-time expression is derived for the acoustic pressure of the reflected wave arising from the incidence of a point-source monopole excited spherical pulse. Depending on the acoustic impedance properties of the boundary, large-amplitude oscillating surface effects can occur. These surface phenomena differ in nature from the true surface waves like the Rayleigh, Scholte, and Stoneley waves in elastodynamics. Illustrative numerical results are presented.
[DOI: 10.1121/1.1766023]

PACS numbers: 43.20.El, 43.20.Bi, 43.20.Px, 43.55.Ev [JJM] Pages: 677–685

I. INTRODUCTION

For a variety of applications, the analysis of the reflection of sound waves, generated by a localized source, from a boundary surface with certain reflection and absorption properties is of importance. In outdoor sound propagation, the boundary can be a natural ground surface. In noise control, it can be a sound-absorbing layer covering a machine part. In architectural acoustics, the boundary can be a part of the sound reflecting and/or scattering structure that serves to realize a particular distribution of sound in, for example, a concert hall. In all these cases, it is of importance to have certain design parameters at one's disposition. This need can, at least partly, be satisfied through the study of certain canonical problems, in which category the analytically solvable ones have the advantage of revealing rather explicitly how the different configurational and material parameters influence the acoustic behavior of a particular structure as a whole.

The present paper performs a study in this category. It discusses the reflection of sound waves generated by an impulsive monopole point source, from a planar boundary with absorptive and dispersive properties. The latter are modeled as a local acoustic impedance relation, i.e., a local relation between the acoustic pressure and the normal component of the particle velocity of the sound wave.[1,2] The absorptive and dispersive properties are expressed via a complex-frequency domain Padé-type expression that guarantees passivity and causality, and in which the parameters can be adjusted to fit measured material reflection data. With the aid of the Cagniard–De Hoop (CdH) method,[3,4] closed-form analytic space-time expressions are obtained for the acoustic pressure in its dependence on the mutual position of a (monopole) source and a (monopole) receiver with respect to the boundary. In the literature,[5–8] much attention is paid to surface effects that show up when source and receiver are close to the boundary and that manifest themselves as large amplitudes in the acoustic pressure (in excess even of the ones associated with the reflection from a rigid boundary) occurring after the arrival of the wave front of the impulsive reflected wave. This phenomenon also shows up in acoustic experiments[9] as well as in the pertaining Finite-Difference Time-Domain method (FDTD) and field emission microscopy Finite Element Method (FEM) studies.[10,11] A careful analysis of the structure of our reflection function shows, however, that this phenomenon is not in the same category as the Rayleigh wave[12] along the planar boundary of a traction free elastic solid, the Scholte wave[3] along the planar fluid/solid interface, or the Stoneley waves[13] along the interface of two different solids. The analytic CdH method employed, further provides the changes in wave shape that the reflected wave undergoes, in their dependence on the parameters[14] occurring in the expression for the boundary's acoustic impedance.

One can argue whether a local impedance-type reaction sufficiently accurately models the presence of the second medium. As the analysis of the two-media problem with point-source excitation shows, the relation between acoustic pressure and normal component of the particle velocity is a nonlocal one of the type of a Dirichlet-to-Neumann map.[15] On the other hand, many studies in the acoustic literature use the local impedance concept. In particular, this holds for the numerical FDTD and FEM studies, where the discretization of a nonlocal Dirichlet-to-Neumann map would destroy the sparsity of the matrix representing the discretized acoustic pressure, while the incorporation of dispersive effects would also imply the incorporation of (noninstantaneous) time-relaxation effects via the relevant temporal convolution integrals. At least the latter phenomena are fully and exactly handled in an approach.

[a]Electronic mail: b.j.kooij@ewi.tudelft.nl

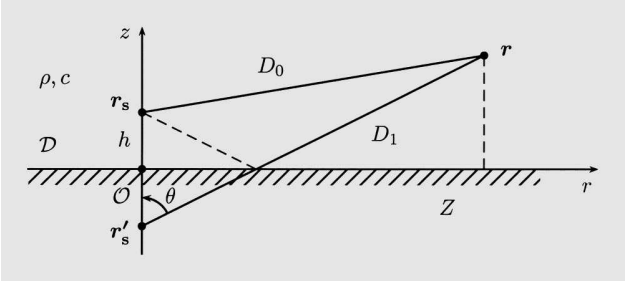

FIG. 1. Half-space configuration where h is the source height. Z is the normalized acoustic impedance transfer function of the planar boundary.

Finally, the analytic expressions obtained can serve as benchmarks in further computational studies based on the discretization of the acoustic wave equations.

II. FORMULATION OF THE PROBLEM

Position in the configuration is specified by the coordinates $\{x,y,z\}$ with respect to an orthogonal, Cartesian reference frame with the origin $\mathcal{O}$. Its base vectors $\{\mathbf{i}_x,\mathbf{i}_y,\mathbf{i}_z\}$ are mutually perpendicular, of unit length each, and they form, in the indicated order, a right-handed system. The position vector is $\mathbf{r}=x\mathbf{i}_x+y\mathbf{i}_y+z\mathbf{i}_z$. The vectorial spatial differentiation operator is $\boldsymbol{\nabla}=\mathbf{i}_x\partial_x+\mathbf{i}_y\partial_y+\mathbf{i}_z\partial_z$. The time coordinate is t; differentiation with respect to time is denoted by ∂_t.

The acoustic wave motion is studied in the half-space $\mathcal{D}=\{-\infty<x<\infty,-\infty<y<\infty,0<z<\infty\}$, which is filled with a fluid with volume density of mass ρ and compressibility κ. The speed of sound waves in it is given by $c=(\rho\kappa)^{-1/2}$. The acoustic pressure $p(\mathbf{r},t)$ and the particle velocity $\mathbf{v}(\mathbf{r},t)$ satisfy the first-order acoustic wave equations

$$\boldsymbol{\nabla}p+\rho\partial_t\mathbf{v}=0, \tag{1}$$

$$\boldsymbol{\nabla}\cdot\mathbf{v}+\kappa\partial_t p=Q(t)\,\delta(\mathbf{r}-\mathbf{r}_s). \tag{2}$$

Here, $Q(t)$ is the volume source density of injection rate (model for the action of a monopole transducer), and $\mathbf{r}_s=\{0,0,h\}$ is the location of the point source. The source starts to act at $t=0$ and prior to this instant the configuration is at rest. Figure 1 shows the configuration. The acoustical properties of the planar boundary are modeled via the linear, time-invariant, local acoustic impedance relation

$$p(x,y,0,t)=-(\rho c)^{-1}Z(t)\overset{(t)}{*}v_z(x,y,0,t), \tag{3}$$

where $\overset{(t)}{*}$ denotes temporal convolution and $Z(t)$ is the acoustic time-domain impedance function of the wall, normalized with respect to the acoustic wave impedance ρc of the fluid. A detailed discussion of the properties of the acoustic impedance is given in Sec. V. The acoustic wave field in the half space is written as the superposition of the incident wave field $\{p^i,\mathbf{v}^i\}$, which is the wave field in the fluid in the absence of the boundary, and the reflected wave field $\{p^r,\mathbf{v}^r\}$, that expresses the action of the reflecting wall, i.e.:

$$\{p,\mathbf{v}\}=\{p^i,\mathbf{v}^i\}+\{p^r,\mathbf{v}^r\}\quad\text{in }\mathcal{D}. \tag{4}$$

III. THE COMPLEX SLOWNESS REPRESENTATION FOR THE ACOUSTIC WAVE FIELDS

The time invariance and the causality of the sound waves are taken into account by the use of the unilateral Laplace transform

$$\{\hat{p},\hat{\mathbf{v}}\}(\mathbf{r},s)=\mathcal{L}[\{p,\mathbf{v}\}(\mathbf{r},t)]=\int_{t=0}^{\infty}\exp(-st)\{p,\mathbf{v}\}(\mathbf{r},t)dt. \tag{5}$$

The Laplace transform parameter s is taken positive and real. Then, according to Lerch's theorem,[16] a one-to-one mapping exists between $\{p,\mathbf{v}\}(\mathbf{r},t)$ and their time-Laplace transformed counterparts $\{\hat{p},\hat{\mathbf{v}}\}(\mathbf{r},s)$. The configuration is initially at rest with the consequence that the transformation property $\partial_t\rightarrow s$ holds. Next, the complex slowness representations for $\{\hat{p},\hat{\mathbf{v}}\}(\mathbf{r},s)$ are introduced as

$$\{\hat{p},\hat{\mathbf{v}}\}(\mathbf{r},s)=\frac{s^2}{4\pi^2}\int_{\alpha=-\infty}^{\infty}d\alpha\int_{\beta=-\infty}^{\infty}\{\tilde{p},\tilde{\mathbf{v}}\}\times(\alpha,\beta,z,s)\exp[-is(\alpha x+\beta y)]d\beta, \tag{6}$$

where α and β are the wave slownesses in the x and y directions, respectively. This representation entails the properties $\partial_x\rightarrow-is\alpha$, $\partial_y\rightarrow-is\beta$. Use of the transforms in Eqs. (1) and (2) yields

$$\begin{bmatrix}\tilde{p}^i\\ \tilde{p}^r\end{bmatrix}(\gamma,z,s)=\frac{\rho\hat{Q}(s)}{2\gamma}\begin{bmatrix}\exp(-s\gamma|z-h|)\\ \tilde{R}(\gamma,s)\exp(-s\gamma D_z)\end{bmatrix}, \tag{7}$$

in which

$$\gamma(\alpha,\beta)=(c^{-2}+\alpha^2+\beta^2)^{1/2} \tag{8}$$

is the wave slowness normal to the boundary with $\mathrm{Re}\{\gamma\}>0$, $D_z=z+h$, and $\tilde{R}$ denotes the slowness-domain reflection coefficient. Using the property, $\tilde{v}_z=-(s\rho)^{-1}\partial_z\tilde{p}$, the impedance boundary condition in the complex slowness domain can be written as

$$\lim_{z\downarrow 0}\partial_z\tilde{p}=\frac{s}{c\hat{Z}(s)}\lim_{z\downarrow 0}\tilde{p}. \tag{9}$$

From Eqs. (7) and (9), it follows that

$$\tilde{R}(\gamma,s)=\frac{c\gamma-1/\hat{Z}(s)}{c\gamma+1/\hat{Z}(s)}. \tag{10}$$

IV. SPACE-TIME EXPRESSIONS FOR THE ACOUSTIC WAVE FIELD CONSTITUENTS

A. Space-time incident wave fields

The expressions for the space-time incident sound waves can be found in De Hoop[17] and are given by

$$p^i(\mathbf{r},t)=\rho\partial_t^2Q(t)\overset{(t)}{*}G^i(\mathbf{r},t), \tag{11}$$

$$\mathbf{v}^i(\mathbf{r},t)=-\partial_tQ(t)\overset{(t)}{*}\boldsymbol{\nabla}G^i(\mathbf{r},t), \tag{12}$$

where

$$G^i(\mathbf{r},t)=\frac{1}{4\pi D_0}H(t-T_0) \tag{13}$$

denotes the incident-wave Green's function for the acoustic pressure. Here, $D_0=(x^2+y^2+|z-h|^2)^{1/2}>0$ is the distance between source and receiver, $T_0=D_0/c$ is the arrival time of the incident wave and $H(t)$ denotes the Heaviside unit step function.

B. Space-time reflected wave fields

The expressions for the reflected acoustic wave fields in the space-time domain are now constructed. With the aid of Eqs. (6) and (7), we first write the expressions for $\hat{p}^r$ and $\hat{v}_z^r$ as

$$\hat{p}^r(\mathbf{r},s)=\rho s^2\hat{Q}(s)\hat{G}^r(\mathbf{r},s), \tag{14}$$

$$\hat{\mathbf{v}}^r(\mathbf{r},s)=-s\hat{Q}(s)\nabla\hat{G}^r(\mathbf{r},s), \tag{15}$$

where

$$\hat{G}^r(\mathbf{r},s)=\frac{1}{4\pi^2}\int_{\alpha=-\infty}^{\infty}d\alpha\int_{\beta=-\infty}^{\infty}\frac{\tilde{R}(\gamma,s)}{2\gamma}\times\exp\{-s[i(\alpha x+\beta y)+\gamma D_z]\}d\beta \tag{16}$$

denotes the reflected-wave Green's function for the acoustic pressure. From Eqs. (14)–(16), it is clear that the determination of the space-time reflected acoustic wave fields has been reduced to finding the space-time domain counterpart of Eq. (16). To this end, we employ the standard procedures in the CdH method.[3,4] The following transformation is carried out first

$$\begin{aligned}\alpha&=-ip\cos(\theta)-q\sin(\theta),\\ \beta&=-ip\sin(\theta)+q\cos(\theta),\end{aligned} \tag{17}$$

which for the vertical slowness leads to $\gamma(q,p)=[\Omega(q)^2-p^2]^{1/2}$, with $\Omega(q)=(c^{-2}+q^2)^{1/2}$. Next, the integration along the imaginary p axis in the complex p plane is replaced by one along the hyperbolic path $pr+\gamma(q,p)D_z=\tau$ with $T_1(q)<\tau<\infty$ where $T_1(q)=D_1\Omega(q)$. Here, $D_1=(x^2+y^2+D_z^2)^{1/2}>0$ is the distance from the image source to the receiver. Subsequently, the transformation

$$q=(\tau^2/D_1^2-c^{-2})^{1/2}\sin(\psi) \tag{18}$$

leads to

$$\hat{G}^r(\mathbf{r},s)=\frac{1}{4\pi D_1}\int_{\tau=T_1}^{\infty}\hat{K}^r(\mathbf{r},\tau,s)\exp(-s\tau)d\tau. \tag{19}$$

Here

$$\hat{K}^r(\mathbf{r},\tau,s)=\frac{2}{\pi}\int_{\psi=0}^{\pi/2}\mathrm{Re}[\tilde{R}(\overline{\gamma},s)]d\psi \tag{20}$$

denotes the reflected-wave kernel function, $T_1=T_1(0)=D_1/c$ is the arrival time of the reflected wave and $\overline{\gamma}(\mathbf{r},\tau,\psi)$ is the slowness after carrying out the indicated transformations. Assuming that $\hat{K}^r(\mathbf{r},\tau,s)$ has a causal time-domain counterpart $K^r(\mathbf{r},\tau,t)$, the space-time reflected-wave Green's function is found as

$$G^r(\mathbf{r},t)=\frac{1}{4\pi D_1}\times\int_{\tau=T_1}^{t}K^r(\mathbf{r},\tau,t-\tau)d\tau H(t-T_1). \tag{21}$$

Finally, the space-time reflected acoustic wave field quantities are obtained as

$$p^r(\mathbf{r},t)=\rho\partial_t^2Q(t)\overset{(t)}{*}G^r(\mathbf{r},t), \tag{22}$$

$$\mathbf{v}^r(\mathbf{r},t)=-\partial_tQ(t)\overset{(t)}{*}\nabla G^r(\mathbf{r},t). \tag{23}$$

The determination of the reflected-wave kernel function, which depends on the impedance of the acoustic wall is discussed in the next section.

V. THE ACOUSTIC IMPEDANCE MODEL AND THE CORRESPONDING REFLECTED-WAVE KERNEL FUNCTION

The acoustic impedance transfer function must satisfy the conditions of linearity, time invariance, causality, and passivity. Accordingly, its complex frequency-domain counterpart must, together with its inverse, be an analytic function of s in $\{\mathrm{Re}(s)>0\}$ and it must take on real values for $\{\mathrm{Re}(s)>0,\mathrm{Im}(s)=0\}$. To meet the condition of partly instantaneous impulse response, $\hat{Z}(s)$ must attain a finite, real, positive limit as $|s|\to\infty$ in $\{\mathrm{Re}(s)\geqslant 0\}$. As in standard linear, time-invariant, causal, passive system theory, we take for $\hat{Z}(s)$ the Padé (2,2) expression

$$\hat{Z}_{(2,2)}(s)=Z_\infty\frac{(s+\alpha_z)(s+\beta_z)}{(s+\alpha_p)(s+\beta_p)}, \tag{24}$$

in which Z_∞, α_z, β_z, α_p, and β_p are adjustable parameters, subject to the conditions $Z_\infty>0$, $\{\alpha_z,\beta_z\}$ either both real and positive or each other's complex conjugate with a positive real part, and $\{\alpha_p,\beta_p\}$ either both real and positive or each other's complex conjugate with a positive real part. In an illustrative numerical result, the values of these coefficients will be matched to frequency-domain ($s=i2\pi f$) reflection measurements applying to the impedance boundary at hand. The time-domain impedance transfer function follows from Eq. (24) as

$$Z_{(2,2)}(t)=Z_\infty[\delta(t)+C_1\exp(-\alpha_pt)H(t)+C_2\exp(-\beta_pt)H(t)], \tag{25}$$

in which

$$\begin{aligned}C_1&=(\alpha_z\beta_z-\alpha_z\beta_p-\beta_z\beta_p+\beta_p^2)/(\alpha_p-\beta_p),\\ C_2&=(\alpha_z\beta_z-\alpha_z\alpha_p-\beta_z\alpha_p+\alpha_p^2)/(\beta_p-\alpha_p).\end{aligned} \tag{26}$$

To proceed with the determination of the reflected wave, $\tilde{R}(\overline{\gamma},s)$ is written as a partial-fraction expression of the type

$$\tilde{R}(\overline{\gamma},s)=\tilde{R}_0(\overline{\gamma})+\frac{\tilde{R}_1(\overline{\gamma})}{s+\tilde{p}_1(\overline{\gamma})}+\frac{\tilde{R}_2(\overline{\gamma})}{s+\tilde{p}_2(\overline{\gamma})}. \tag{27}$$

From Eqs. (10) and (24), the coefficients in this expression are found as

$$\tilde{R}_0(\overline{\gamma})=a_2/b_2,\quad \tilde{R}_1(\overline{\gamma})=d_1/2+D^{-1}(d_1e_1/2-d_0),$$

$$\tilde{R}_2(\overline{\gamma}) = d_1/2 + D^{-1}(d_0 - d_1 e_1/2), \tag{28}$$
$$\tilde{p}_1(\overline{\gamma}) = (e_1 + D)/2, \quad \tilde{p}_2(\overline{\gamma}) = (e_1 - D)/2,$$

where

$$D(\overline{\gamma}) = (e_1^2 - 4e_0)^{1/2}, \quad d_0(\overline{\gamma}) = a_0/b_2 - b_0 a_2/b_2^2,$$
$$d_1(\overline{\gamma}) = a_1/b_2 - b_1 a_2/b_2^2, \quad e_0(\overline{\gamma}) = b_0/b_2,$$
$$e_1(\overline{\gamma}) = b_1/b_2, \quad a_0(\overline{\gamma}) = c\overline{\gamma}Z_\infty \alpha_z \beta_z - \alpha_p \beta_p,$$
$$a_1(\overline{\gamma}) = c\overline{\gamma}Z_\infty(\alpha_z + \beta_z) - (\alpha_p + \beta_p), \tag{29}$$
$$a_2(\overline{\gamma}) = c\overline{\gamma}Z_\infty - 1, \quad b_0(\overline{\gamma}) = c\overline{\gamma}Z_\infty \alpha_z \beta_z + \alpha_p \beta_p,$$
$$b_1(\overline{\gamma}) = c\overline{\gamma}Z_\infty(\alpha_z + \beta_z) + (\alpha_p + \beta_p),$$
$$b_2(\overline{\gamma}) = c\overline{\gamma}Z_\infty + 1.$$

Use of Eq. (27) in Eq. (20) yields

$$\hat{K}^r(\mathbf{r},\tau,s) = \frac{2}{\pi}\int_{\psi=0}^{\pi/2} \mathrm{Re}\left[\tilde{R}_0 + \frac{\tilde{R}_1}{(s+\tilde{p}_1)} + \frac{\tilde{R}_2}{(s+\tilde{p}_2)}\right] d\psi, \tag{30}$$

from which the space-time counterpart follows as:

$$K^r(\mathbf{r},\tau,t) = \frac{2}{\pi}\int_{\psi=0}^{\pi/2} \mathrm{Re}[\tilde{R}_0 \delta(t) + \tilde{R}_1 \exp(-\tilde{p}_1 t)H(t) + \tilde{R}_2 \exp(-\tilde{p}_2 t)H(t)]d\psi. \tag{31}$$

If in the integration on the right-hand side values of ψ are met where $D(\overline{\gamma}) = 0$, the last two terms do blow up, but their sum attains a finite limit, as inspection of Eqs. (28) and (29) learns. This difficulty is circumvented by keeping, in the numerical procedure, always the last two terms together.

The solution for the kernel function is now complete and the space-time Green's function for the reflected acoustic pressure is found with Eq. (21). The delta function in Eq. (31) yields an instantaneous response in the reflected-wave Green's function, while the remaining terms, containing the exponential functions, start with zero values at the arrival time, and lead to the occurrence of a dispersive tail.

VI. SPECIAL CASES

In this section, we present expressions for the Green's function in some special cases. These are A: the arrival-time value, B: the case of source and receiver both placed on the boundary, C: the case of source and receiver aligned normal to the boundary.

A. Green's function at the arrival time

At the arrival time, $t = T_1$, the τ integral in Eq. (21) vanishes and only the delta function in Eq. (31) with $\tilde{R}_0$ as coefficient contributes to the reflected wave field value. $\tilde{R}_0$ depends on Z_∞ only and, hence, the relaxation properties of the boundary material do not influence the reflected wave at the early time. In terms of the angle θ, which is indicated in Fig. 1, the space-time reflected-wave Green's function for the acoustic pressure at the arrival time is

$$G^r(\theta(\mathbf{r}), t = T_1) = \frac{1}{4\pi D_1} R(\theta), \tag{32}$$

where

$$R(\theta) = \frac{\cos(\theta) - 1/Z_\infty}{\cos(\theta) + 1/Z_\infty}. \tag{33}$$

At normal incidence, we have $R(0) = (Z_\infty - 1)/(Z_\infty + 1)$, while at grazing incidence $R(\pi/2) = -1$. Another observation is that the numerator in Eq. (33) becomes zero when $\tan(\theta_B) = (Z_\infty^2 - 1)^{1/2}$. This occurs only for $Z_\infty \geqslant 1$, in which case θ_B is the Brewster angle, known from optics.

B. Source and receiver both on the boundary

For the case where both source and receiver are placed on the boundary, $D_z = 0$, we can not treat the incident and reflected wave fields separately. Therefore, we consider the total-wave Green's function for the acoustic pressure, whose complex slowness representation is given by (cf. Eqs. (16) and (17)):

$$\hat{G}(\mathbf{r},s)|_{D_z=0} = \frac{1}{4\pi^2 i}\int_{q=0}^{\infty} dq \int_{p=-i\infty}^{i\infty} \frac{1 + \tilde{R}(\gamma,s)}{\gamma} \times \exp(-spr)dp. \tag{34}$$

Replacing the integration along the imaginary p axis by a loop integral along the branch cut on the positive real p axis, which procedure is admissible since Jordan's lemma and Cauchy's theorem apply, the total-wave Green's function for the acoustic pressure is obtained as

$$\hat{G}(\mathbf{r},s)|_{D_z=0} = \frac{1}{2\pi r}\int_{\tau=T_1}^{\infty} \hat{K}(r,\tau,s)\exp(-s\tau)d\tau, \tag{35}$$

where

$$\hat{K}(\mathbf{r},\tau,s)|_{D_z=0} = \frac{2}{\pi}\int_{\psi=0}^{\pi/2} \frac{|\overline{\gamma}|^2}{|\overline{\gamma}|^2 + [\hat{Z}(s)c]^{-2}} d\psi \tag{36}$$

denotes the kernel function and $T_1 = r/c$ is the arrival time in this special case. After some elaboration the kernel function can be written in the form

$$\hat{K}(\mathbf{r},\tau,s)|_{D_z=0} = 1 - [1 + \hat{Z}(s)^2(\tau^2/T_1^2 - 1)]^{-1/2}. \tag{37}$$

For two special cases of this configuration, the transformation back to the time domain can be carried out analytically rather than numerically. The first one occurs when the acoustic impedance can be modeled as a Padé (0,0) expression, $\hat{Z}_{(0,0)}(s) = Z_\infty$, i.e., when no boundary relaxation effects occur. Then

$$G(\mathbf{r},t)|_{D_z=0} = \frac{1}{2\pi r}[1 - (1 + u^2)^{-1/2}]H(t - T_1), \tag{38}$$

where $u(r,t) = Z_\infty(t^2/T_1^2 - 1)^{1/2}$. This function decreases monotonically with increasing r and t and, hence, no peaked surface effects do occur. The second case amounts to a (1,1) Padé representation of the acoustic impedance

$$\hat{Z}_{(1,1)}(s)=Z_\infty\frac{(s+\alpha_z)}{(s+\alpha_p)}, \tag{39}$$

which case covers a large class of wool felts and grass grounds.[10] With the aid of Eqs. (35), (37), and (39), the space-time total-wave Green's function becomes

$$G(\mathbf{r},t)|_{D_z=0}=\frac{1}{2\pi r}H(t-T_1) - \frac{1}{\pi}\int_{\tau=T_1}^{\infty}\mathcal{L}^{-1}\left[\frac{(s+\alpha_p)\exp(-s\tau)}{(a_2s^2+a_1s+a_0)^{1/2}}\right]d\tau, \tag{40}$$

with

$$a_0(r,\tau)=\alpha_p^2+\alpha_z^2u^2,$$
$$a_1(r,\tau)=2(\alpha_p+\alpha_zu^2),\quad a_2(r,\tau)=1+u^2, \tag{41}$$

where $u=u(r,\tau)$. Using

$$\mathcal{L}^{-1}\left[\frac{\exp(-s\tau)}{\sqrt{s^2+a^2}}\right]=J_0[a(t-\tau)]H(t-\tau),\quad a\geqslant 0, \tag{42}$$

where $J_0(t)$ is the Bessel function of the first kind and order zero, the space-time total-wave Green's function for the acoustic pressure is obtained as

$$G(\mathbf{r},t)|_{D_z=0} =\frac{1}{2\pi r}\left[1-\frac{1}{\sqrt{a_2(r,t)}}-\int_{\tau=T_1}^{t}\frac{\exp[-v(t-\tau)]}{\sqrt{a_2(r,\tau)}} \times L\{J_0[w(t-\tau)]\}d\tau\right]H(t-T_1), \tag{43}$$

where

$$v(r,\tau)=a_1/(2a_2),\quad w(r,\tau)=|\alpha_z-\alpha_p|u/a_2\geqslant 0, \tag{44}$$

and L given by $L(r,t,\tau)=\partial_t+\alpha_p-v$. The time derivative acting on the Bessel function can be circumvented by using the Bessel functions property: $J_1(t)=-\partial_tJ_0(t)$. The argument of this Bessel function in Eq. (43) is always nonnegative and real. As a result, the part of the total-wave Green's function containing the Bessel function shows an oscillating behavior.

Equation (43) is in agreement with the result obtained by Donato[8] through a different procedure. In his paper, Donato used the Padé (0,1) representation for this special case.

C. Source and receiver aligned normal to the boundary

For the case of source and receiver aligned normal to the impedance boundary, we proceed differently and first introduce new variables of integration in Eq. (16), *viz.* $\alpha=\nu\cos(\phi)$ and $\beta=\nu\sin(\phi)$. Using the rotational symmetry, the reflected-wave Green's function for the acoustic pressure now becomes

$$\hat{G}^r(\mathbf{r},s)|_{r=0}=\frac{1}{4\pi}\int_{\nu=0}^{\infty}\frac{\nu\tilde{R}(\gamma,s)}{\gamma}\exp(-s\gamma D_z)d\nu, \tag{45}$$

where $\gamma=(c^{-2}+\nu^2)^{1/2}$. After introducing $\tau=\gamma D_z$, the result is

$$\hat{G}^r(\mathbf{r},s)|_{r=0}=\frac{1}{4\pi D_z}\int_{\tau=T_1}^{\infty}\tilde{R}(\tau/D_z,s)\exp(-s\tau)d\tau, \tag{46}$$

where $T_1=D_z/c$ is the arrival time. The space-time reflected-wave Green's function for the acoustic pressure then follows as:

$$G^r(\mathbf{r},t)|_{r=0}=\frac{1}{4\pi D_z}\int_{\tau=T_1}^{t}\tilde{R}(\tau/D_z,t-\tau)d\tau H(t-T_1). \tag{47}$$

VII. SURFACE EFFECTS

As a result of the conditions laid upon γ and $\hat{Z}(s)$ (positive real parts for real, positive s), the denominator of $\tilde{R}(\gamma,s)$ as it occurs in Eq. (16) is free from zeros. This implies that no true surface waves like the Rayleigh wave,[12] Scholte wave,[3] and Stoneley waves[13] in elastodynamics, where such zeroes do occur in the pertaining complex slowness domain reflection coefficients, exist. However, large surface effects in the acoustic pressure have been reported if both source and receiver are close to the boundary, depending on the values of the parameters determining $\hat{Z}(s)$. In the frequency domain, an impedance showing this behavior is found to have a resistive part that is small compared with a (negative) reactance part.[6–8] Such a type of impedance can be modeled as a Padé (1,1) representation of the kind in Eq. (39). For source and receiver on the boundary, Eqs. (43) and (44) provide the Green's function. The Bessel function in it shows an oscillating behavior. Its argument is proportional to $|\alpha_z-\alpha_p|$ which is large as $\alpha_z\gg\alpha_p$ (the other possibility, $\alpha_z\ll\alpha_p$, has not been encountered in the literature). To what degree the oscillations in the Bessel function finally show up in the Green's function is, due to the integration with respect to τ, difficult to say.

The acoustic pressure is mathematically the temporal convolution of the time signature of the source with the Green's function. Convolution is, however, a smoothing process whose final result may mask many interesting details in the Green's function, the latter being determined by the configurational and material parameters only. Therefore, we discuss and do show in the next section the Green's functions for three types of physical impedances and we will reveal interesting features in the reflected sound waves that are only mentioned qualitatively in the experimental literature.

VIII. NUMERICAL RESULTS

For three acoustic impedance models, the space-time reflected-wave Green's function for the acoustic pressure will be presented. The results for the three impedance models are discussed separately later.

A. Instantaneously reacting impedance boundary (Padé (0,0) complex frequency domain representation)

For the instantaneously reacting impedance boundary, we have the Padé (0,0) representation: $\hat{Z}_{(0,0)}(s)=Z_\infty$. For

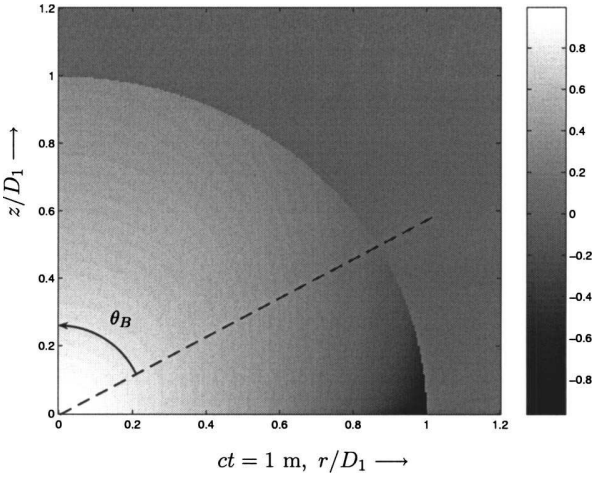

FIG. 2. Normalized density plot of G^r at $ct/h=330$, where $h>0$, for an instantaneously reacting wall impedance: $Z=2$. The Brewster angle is $\theta_B=60°$. No surface phenomenon appears at large offsets parallel to the boundary.

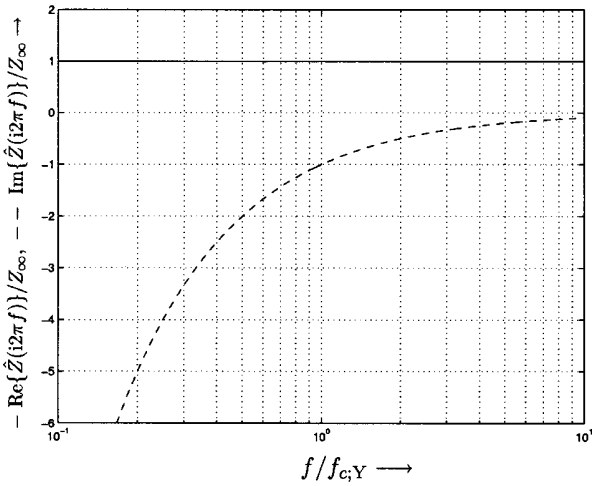

FIG. 3. Frequency response of the mineral wool acoustic impedance model. The acoustic admittance corner frequency is $f_{c;Y}=1.06$ kHz.

this type of boundary, no large amplitude oscillating surface effects are expected, a result confirmed by the literature.[6–8] For $Z=2$, Fig. 2 shows a density plot of the normalized reflected-wave Green's function, $4\pi D_1 \times G^r$ (normalization with respect to the reflected-wave Green's function in the rigid boundary case, $Z\rightarrow\infty$), at $ct/h=330$ where $ct=1$ m and $h>0$. Note that the arrival-time response of G^r vanishes at the Brewster angle $\theta_B=60°$. The plot is in agreement with the results of Ingard.[2] It is observed that the reflected-wave Green's function is less than unity everywhere in the configuration.

B. Mineral wool acoustic impedance boundary (Padé (1,1) complex frequency domain representation)

A 50 mm mineral wool with hard backing can be modeled as a Padé (1,1) representation (Eq. (39)). From the literature,[18] the following values are taken $Z_\infty=1$, $\alpha_z=6700\,\mathrm{s}^{-1}$, $\alpha_p=0$. The corresponding acoustic admittance relaxation time is $\tau_{\mathrm{rel}}=940\,\mu$s and the spectral diagram acoustic admittance corner frequency is $f_{c,Y}=1.06$ kHz. Figure 3 shows the real and imaginary parts of the frequency-domain mineral wool acoustic impedance model, $\hat{Z}_{(1,1)}(i2\pi f)$. Figures 4(a)–(c) show density plots for the normalized reflected-wave Green's function at $ct/h=330$ where

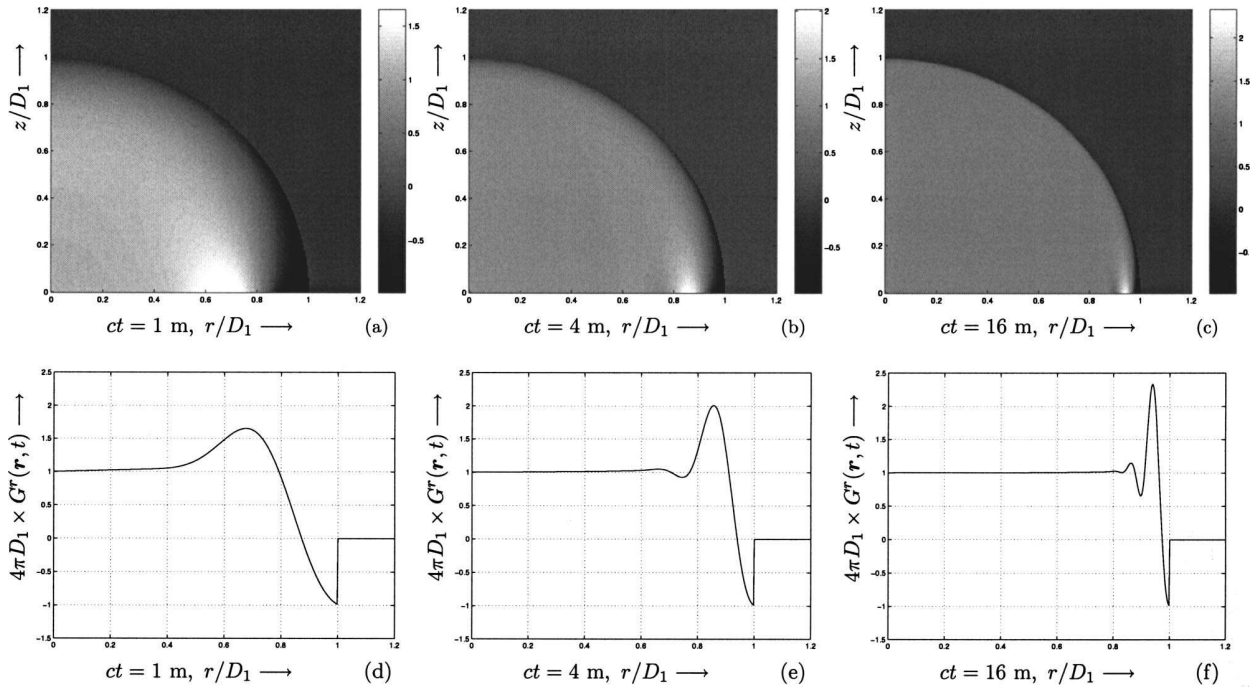

FIG. 4. (a)–(c) Normalized density plot of G^r in the mineral wool acoustic impedance model with $ct/h=330$ where $ct=\{1,4,16\}$ m. Oscillating surface effects occur at large offsets parallel to the boundary. The maximum value exceeds the value of the Green's function in the rigid boundary case. (d)–(f) The corresponding time snaps at source height h.

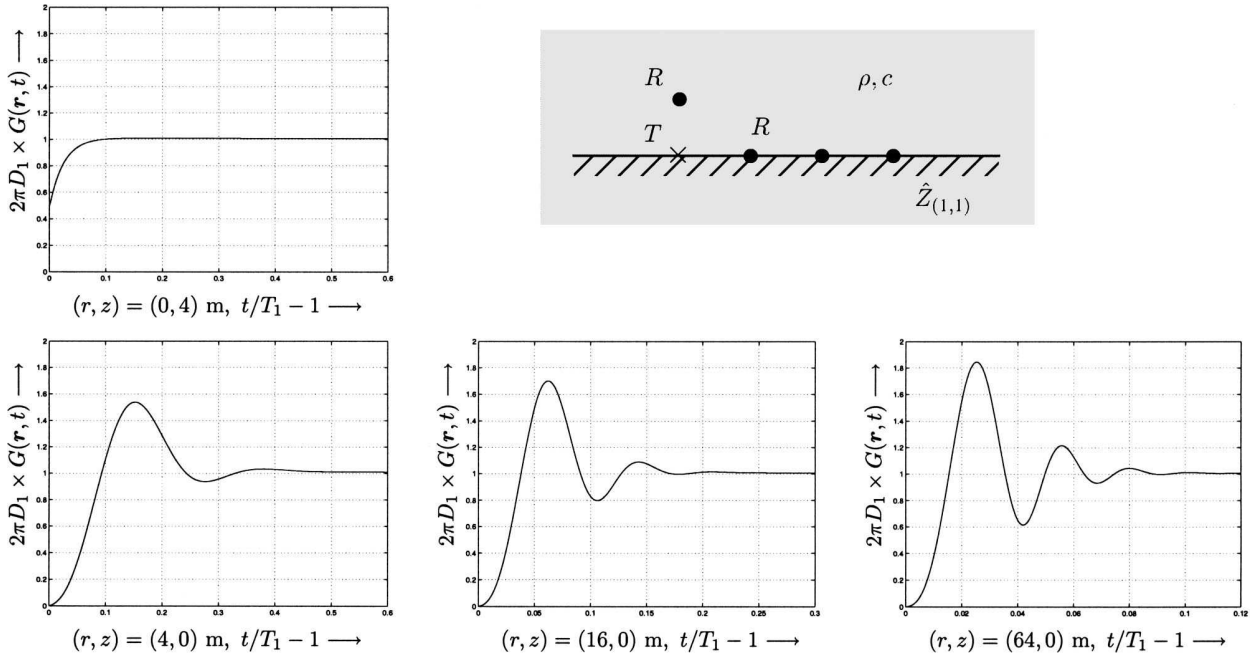

FIG. 5. Time traces of the normalized total-wave Green's function in the mineral wool acoustic impedance model. Time oscillations occur at large offsets parallel to the boundary. The Green's function $G \rightarrow 1/2\pi D_1$ as $t \rightarrow \infty$.

$ct = \{1,4,16\}$ m, respectively. The relevant amplitude at source height h are depicted in Figs. 4(d)–(f). Large amplitude oscillatory surface effects are observed at large offsets parallel to the boundary. The maximum value of the Green's function exceeds the value of the rigid boundary case Green's function, a phenomenon which has also been reported by Diagle *et al.*[7] It is noted that this phenomenon is entirely due to the absorptive and dispersive behavior of the boundary impedance. Furthermore, its magnitude depends on the actual values of the parameters employed. Finally, some time traces are shown in Fig. 5.

C. NASA Langley CT73 acoustic impedance (Padé (2,2) complex frequency domain representation)

The NASA Langley CT73 flow impedance tube with a constant depth ceramic tubular liner is considered and modeled as a Padé (2,2) expression. The data from frequency-response measurements are taken from Özyörük *et al.*[19] The first parameter to be estimated is the arrival time acoustic impedance, which is taken as $Z_\infty = 2$. The relaxation parameters in Eq. (24) are found by fitting the acoustic impedance model to the measured data spectrum in the frequency interval $f \in (0.5,3.0)$ kHz. The obtained values in the $\hat{Z}_{(2,2)}(s)$ impedance model are: $Z_\infty = 2$, $\alpha_z = 1000\pi\ \mathrm{s}^{-1}$, $\beta_z = 5200\pi\ \mathrm{s}^{-1}$, $\alpha_p = 1300\pi + i3400\pi\ \mathrm{s}^{-1}$ and $\beta_p = 1300\pi - i3400\pi\ \mathrm{s}^{-1}$. The acoustic impedance damped natural frequency is $f_{d;Z} = 1.7$ kHz. Figure 6 shows the real and imaginary parts of the frequency-domain Langley CT73 acoustic impedance model, $\hat{Z}_{(2,2)}(i2\pi f)$. Figures 7(a)–(c) show density plots for the normalized reflected-wave Green's function at $ct/h = 330$ where $ct = \{1,4,16\}$ m, respectively. The relevant amplitude at source height h are depicted in Figs. 7(d)–(f). Small amplitude oscillatory surface effects occur in the Green's function, which are, however, hardly detectable in the (measured) acoustic pressure. It is noted that the Green's function is less than unity in all space. In Fig. 8, finally, some time traces at source height and different horizontal offsets are depicted to show the small amplitude transient oscillations in the reflected-wave Green's function.

IX. DISCUSSION OF THE RESULTS

In Sec. VIII B, we used the same impedance model as in the Refs. 6–8 where it can lead to large amplitude surface effects. In the present analysis, oscillations in the reflected-wave Green's function do occur in space and time. The maximum amplitude of the oscillations exceeds the value of the rigid boundary Green's function for the situations where source and receiver are close to the impedance boundary.

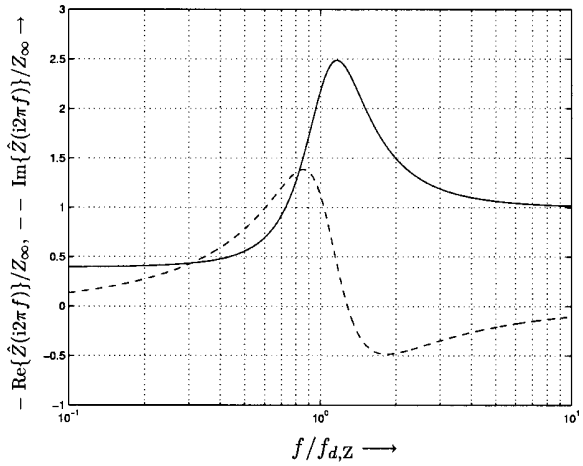

FIG. 6. Frequency response of the Langley CT73 acoustic impedance model. The acoustic impedance damped natural frequency is $f_{d;Z} = 1.7$ kHz.

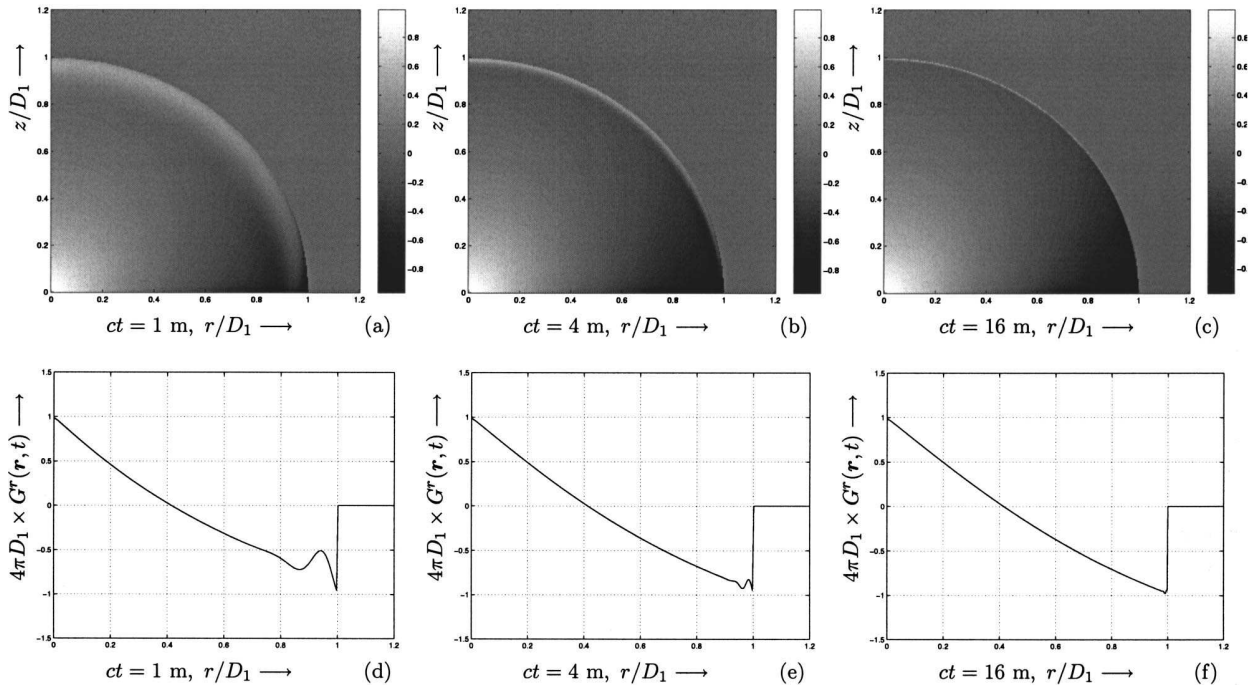

FIG. 7. (a)–(c) Normalized density plots of G^r in the Langley CT73 acoustic impedance model with $ct/h = 330$, where $ct = \{1,4,16\}$ m. No oscillations with large amplitudes in the Green's function occur at large horizontal offsets parallel to the boundary. (d)–(f) The corresponding time snaps at source height.

When the source and receiver are placed away from the boundary, the magnitude of the oscillations decreases gradually.

In Sec. VIII C, we modeled the Langley CT73 acoustic impedance with a Padé (2,2) expression. Small amplitude oscillations do occur in the reflected-wave Green's function, but they are hardly detectable in measurements.

As far as the agreement with the literature is concerned, surface effects in the form of oscillatory features do occur. The magnitude of the oscillations depends on the parameters in the impedance model. Other experiments with the mineral wool impedance model, where only Z_∞ is increased, i.e., increasing the resisitive part of the frequency-domain acoustic impedance, while retaining the magnitude of the reactance part, show that the amplitude of the oscillations decreases. This experimental finding, together with the remarks in Sec. VII are indicative for the presence of large amplitude oscillatory surface effects in the cases where the frequency-domain acoustic impedance has a large negative reactance part as compared with its positive resistive part. This spectral property holds for the mineral wool impedance model, but not for the Langley CT73 impedance model as observed from Figs. 3 and 6.

X. CONCLUSIONS

Closed-form time-domain expressions are derived for the reflected sound waves above an absorptive and dispersive planar boundary. A Padé type expression has been used to model the acoustic impedance. This choice makes the partial-fraction decomposition of the reflection coefficient possible with the consequence that the transformation back to the time domain can be carried out analytically.

The surface wave phenomenon above the impedance boundary has been discussed in Sec. VII. No surface waves like the Rayleigh wave, the Scholte wave, and the Stoneley waves in elastodynamics, are argued to exist. However, oscillatory surface effects do occur due to the absorptive and

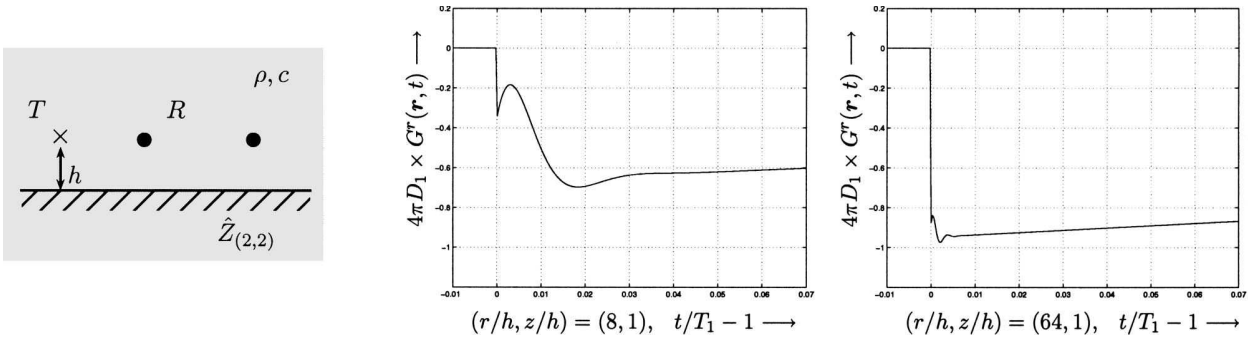

FIG. 8. Time traces of the normalized reflected-wave Green's function in the Langley CT73 acoustic impedance model at source height and different horizontal offsets. The Green's function $G^r \to 1/4\pi D_1$ as $t \to \infty$.

dispersive properties of the boundary material. These oscillatory features are large in magnitude only if the frequency-domain acoustic impedance possesses the property of a large negative reactance part as compared with its positive resistive part.

[1] P. M. Morse and K. U. Ingard, *Theoretical Acoustics* (McGraw Hill, New York, 1968), pp. 259–266.

[2] K. U. Ingard, "On the reflection of a spherical sound wave from an infinite plane," J. Acoust. Soc. Am. **23**, 329–335 (1951).

[3] A. T. De Hoop and J. H. M. T. van der Hijden, "Generation of acoustic waves by an impulsive point source in a fluid/solid configuration with a plane boundary," J. Acoust. Soc. Am. **75**, 1709–1715 (1984).

[4] A. T. de Hoop, "Reflection and transmission of a transient, elastic line-source excited SH-wave by a planar, elastic bounding surface in a solid," Int. J. Solids Struct. **39**, 5379–5391 (2002).

[5] S. R. Wenzel, "Propagation of waves along an impedance boundary," J. Acoust. Soc. Am. **55**, 956–963 (1974).

[6] S. I. Thomasson, "Reflection of waves from a point source by an impedance boundary," J. Acoust. Soc. Am. **59**, 780–785 (1976).

[7] R. J. Donato, "Propagation of a spherical wave near a plane boundary with a complex impedance," J. Acoust. Soc. Am. **60**, 34–39 (1976).

[8] R. J. Donato, "Spherical-wave reflection from a boundary of reactive impedance using a modification of Cagniard's method," J. Acoust. Soc. Am. **60**, 999–1002 (1976).

[9] G. A. Daigle, M. R. Stinson, and D. I. Havelock, "Experiments on surface waves over a model impedance plane using acoustical pulses," J. Acoust. Soc. Am. **99**, 1993–2005 (1996).

[10] H. B. Ju and K. Y. Fung, "Time-domain simulation of acoustic sources over an impedance plane," J. Comput. Acoust. **10**, 311–329 (2002).

[11] B. Van den Nieuwenhof and J. P. Coyette, "Treatment of frequency-dependent admittance boundary conditions in transient acoustic finite/infinite-element models," J. Acoust. Soc. Am. **110**, 1743–1751 (2001).

[12] J. D. Achenbach, *Wave Propagation in Elastic Solids* (Elsevier Science, New York, 1999).

[13] L. Cagniard, *Reflection and Refraction of Progressive Seismic Waves* (McGraw-Hill, New York, 1962), pp. 47–50, 244. E. A. Flinn and C. H. Dix, *Réflexion et Réfraction des Ondes Séismiques Progressives* (Gauthier-Villars, Paris, 1939), translation and revision of L. Cagniard.

[14] K. Attenborough, "Ground parameter information for propagation modeling," J. Acoust. Soc. Am. **92**, 418–427 (1992).

[15] M. Lassas, M. Cheney, and G. Uhlmann, "Uniqueness for a wave propagation inverse problem in a half space," Inverse Probl. **14**, 679–684 (1998).

[16] D. V. Widder, *The Laplace Transform* (Princeton University Press, Princeton, NJ, 1946), pp. 63–65.

[17] A. T. de Hoop, *Handbook of Radiation and Scattering of Waves* (Academic, San Diego, 1995).

[18] L. C. Sutherland and G. A. Daigle, "Atmospheric sound propagation," in *Handbook of Acoustics*, edited by M. J. Crocker (Wiley, New York, 1998), pp. 305–329.

[19] Y. Özyörük and L. N. Long, "Time-domain impedance boundary conditions for computational aeroacoustics," J. Comput. Acoust. **5**, 277–296 (1997).